




RESEARCH ARTICLE | JANUARY 17 2024

# Single-board low-noise fluxgate magnetometer

T. Dyer ; P. F. Griffin ; E. Riis 



*J. Appl. Phys.* 135, 034501 (2024)

<https://doi.org/10.1063/5.0175418>



CrossMark



**APL Quantum**  
Bridging fundamental quantum research with technological applications

**Now Open for Submissions**  
No Article Processing Charges (APCs) through 2024

**Submit Today**



# Single-board low-noise fluxgate magnetometer

Cite as: J. Appl. Phys. **135**, 034501 (2024); doi: [10.1063/5.0175418](https://doi.org/10.1063/5.0175418)

Submitted: 6 September 2023 · Accepted: 22 December 2023 ·

Published Online: 17 January 2024



T. Dyer,<sup>a)</sup> P. F. Griffin, and E. Riis

## AFFILIATIONS

Department of Physics, SUPA, University of Strathclyde, Glasgow G4 0NG, United Kingdom

<sup>a)</sup>Author to whom correspondence should be addressed: [terry.dyer@strath.ac.uk](mailto:terry.dyer@strath.ac.uk)

## ABSTRACT

Low-noise fluxgate magnetometers are normally comprised of three separate devices: a power supply, the sensor head/electronics and an analog-to-digital converter (ADC). This paper presents a parallel rod fluxgate magnetometer in a single printed circuit board of size =  $5 \times 12$  cm, weight = 45 g, and sensor head average power dissipation = 40 mW. The open-loop noise spectral density =  $5 pT_{rms}/\sqrt{\text{Hz}} @ 1 \text{ Hz}$ , competitive with state-of-the-art devices. This is realized using a new amorphous wire core material and programmable mixed-signal electronics with low amplifier and ADC noise. We have compared the sensor performance to a low-noise observatory magnetometer and found sub-nT correlation when tracking the Y (East-West) component of the Earth's geomagnetic field.

© 2024 Author(s). All article content, except where otherwise noted, is licensed under a Creative Commons Attribution (CC BY) license (<http://creativecommons.org/licenses/by/4.0/>). <https://doi.org/10.1063/5.0175418>

## I. INTRODUCTION

Low-noise fluxgate magnetometers<sup>1-3</sup> are vector sensors that can operate over a wide dynamic range, e.g., 6 pT–60  $\mu$ T (140 dB). They are established in several scientific fields, including geomagnetism,<sup>4</sup> space exploration,<sup>5,6</sup> and navigation.<sup>7</sup> Looking forward, current sensing presents a potential market growth opportunity, e.g., as a diagnostic tool to optimize the safety, performance, and lifetime of electric vehicle (EV) batteries.<sup>8-10</sup> The current sensing market has recently seen the introduction of a chip-scale fluxgate magnetometer,<sup>11</sup> enabling new applications such as current imaging at the mm scale. However, a significant limitation is its high noise level, approximately three orders of magnitude greater than the best commercially available fluxgate magnetometers.

In many fluxgate implementations, magnetically soft ferromagnetic wires are employed as the core material. Optimization of the core properties,<sup>12</sup> together with the electronic circuits, is key to building a low-noise sensor. The sensor head has two main design types. Most popular is the parallel fluxgate,<sup>13</sup> and state-of-the-art devices exhibit noise densities of  $3 - 4 pT_{rms}/\sqrt{\text{Hz}} @ 1 \text{ Hz}$ .<sup>14</sup> The lowest fluxgate noise levels,  $< 1 pT_{rms}/\sqrt{\text{Hz}} @ 1 \text{ Hz}$ , have been reported using a fundamental mode open-loop orthogonal design,<sup>15,16</sup> enabling real-time human magnetocardiography (MCG) in an un-shielded environment.<sup>14</sup> This recent research finding indicates the potential for fluxgate magnetometers to compete in bio-medical applications with technologies, such as

super-conducting quantum interference devices (SQUIDs) and atomic magnetometers.<sup>17</sup>

While most fluxgates are operated in a closed-loop feedback mode,<sup>18</sup> open-loop can offer lower noise and crosstalk over a reduced linear range due to the absence of the compensation coil drive.<sup>14</sup> In un-shielded operation, the external field seen by the core can be nulled by orienting the fluxgate axis of sensitivity parallel to the Y (East-West) component of the Earth's geomagnetic field.

The aim of this work is to develop a single-board low-noise fluxgate magnetometer, containing all components needed to output digital magnetic flux density data, and to use geomagnetic field testing to demonstrate its performance. We use commercially available amorphous wire cores and integrated circuits (ICs) in a mixed-signal printed circuit board (PCB).

## II. FLUXGATE MAGNETOMETER FABRICATION

### A. Sensor head

Our fluxgate magnetometer uses a single-axis parallel rod Vacquier design<sup>13,18</sup> (Fig. 1). One advantage of this design is the large geometrical anisotropy, which offers high resistance to cross fields. The core elements are CoFeSiB 0.1 mm diameter, 15 mm long amorphous wires (100DC2T from Aichi-Steel<sup>19</sup>) with extremely low magnetic hysteresis, coercivity  $H_c = 4 \text{ A/m}$ , and saturation magnetization flux density  $B_{sat} = 0.6 \text{ T}$ . To the best of our knowledge, this is the first reported use of this core material in a fluxgate implementation. Excitation and sense coils are formed

18 January 2024 16:40:50

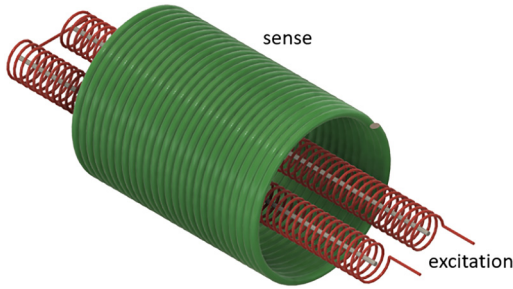


FIG. 1. Schematic of the basic sensor head (supporting structures not shown). The two parallel wire cores are driven by counter-wound excitation coils, and the fluxgate is detected via a single sense coil.

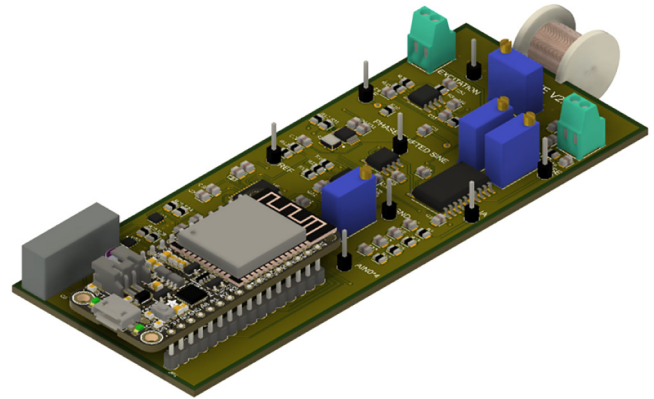


FIG. 3. Prototype PCB CAD image including on board micro-controller and sensor head. The sensor head (Fig. 1) is constructed around a 3D printed former (LEDO 6060 Resin) mounted on the PCB edge. PCB size =  $5 \times 12$  cm and weight = 45 g. Power and data share a 5V USB cable connected to the micro-controller.

from 0.1 and 0.2 mm diameter enameled Cu wire, respectively. The number of excitation coil turns  $N_e = 100 \times 2$  and sense coil turns  $N_s = 600$ .

### B. Sensor electronics

We use the conventional method of measuring the fluxgate sense coil second harmonic ( $2f$ ) signal. A high-level schematic of the open-loop sensor electronics is shown in Fig. 2 and a CAD image of the prototype PCB in Fig. 3.

1f and 2f phase-locked signals are generated by a programmable multi-channel radio frequency (RF) generator/phase-locked loop (PLL). The 1f signal drives the power amplifier to the excitation coils, and the 2f signal is used as the reference input to the

synchronous demodulator. A low-pass filter with cut-off frequency ( $-3$  dB) = 100 Hz follows the synchronous demodulator. A phase-shifter enables adjustment of the phase difference between the 1f and 2f signals. The 2f fluxgate sense coil signal is synchronously demodulated back to DC, and this DC signal is then sampled by a bipolar 32-bit  $\Sigma - \Delta$  analog-to-digital converter (ADC).

The 32-bit ADC has an adjustable sample rate (5 Hz–10 kHz) and digital filtering options for bandwidth tuning and noise

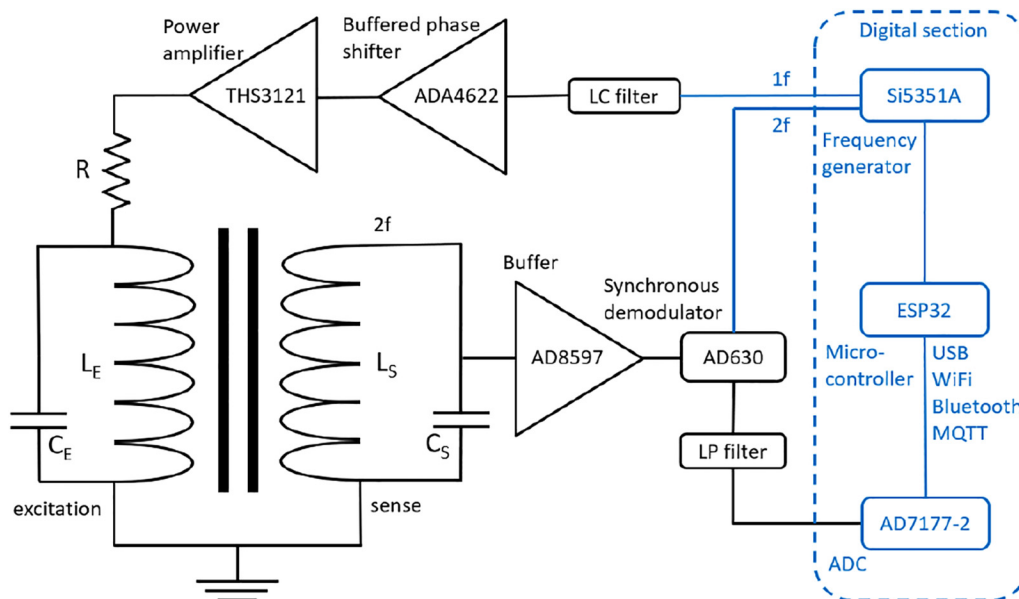
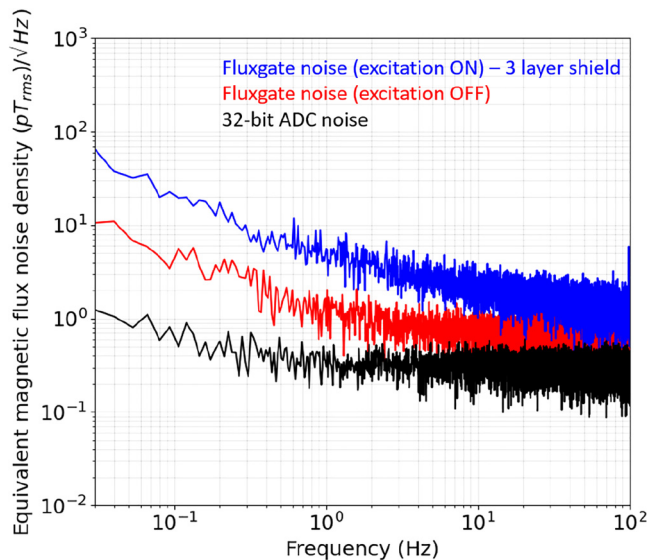


FIG. 2. Open-loop fluxgate magnetometer high-level schematic. The frequency generator and ADC are firmware programmable through an on board micro-controller.

18 January 2024 16:40:50



**FIG. 4.** Magnetic flux noise spectral density of the fluxgate magnetometer inside a three-layer shield (blue line). Also shown is the equivalent magnetic flux noise spectral density with the fluxgate connected and excitation switched off in software (red line) and for the 32-bit ADC only (black line).

reduction. The effective bit resolution depends on the sample rate and digital filter used. The magnetic flux density noise results presented in this paper use a 200 Hz sample rate and digital filtering for an effective resolution of 24 bits. Geomagnetic field data are taken at a 5 Hz sample rate, digitally filtered, and further averaged to obtain an effective resolution of 28 bits.

The excitation coil circuit is designed to drive the cores deep into saturation, reducing permeating effects and noise while

maintaining low power consumption.<sup>20,21</sup> The sensor head average power dissipation = 40 mW. A resonant LC circuit provides band-pass filtering and parametric amplification of the  $2f$  fluxgate sense coil signal. The resonant LC circuit is formed by tuning capacitor  $C_S$  in parallel with the sense coil  $L_S$ . The  $2f$  frequency = 30 kHz is chosen to match the resonant frequency and can be fine tuned in software to maximize parametric amplification thereby reducing amplifier noise. The settling time of the tuned fluxgate output is less than the sampling time of the ADC. The tuned fluxgate output is buffered to avoid loading the resonant circuit.

An on board micro-controller manages the fluxgate magnetometer operation and sends digital magnetic flux density data to a computer USB port. The PCB can also be mains powered using a micro-USB charger or battery powered. Data are then sent by the micro-controller over WiFi or Bluetooth by Message Queue Telemetry Transport (MQTT) to a cloud server. The cloud server provides real-time data plotting options in addition to data storage.

### III. FLUXGATE MAGNETOMETER CHARACTERIZATION

The fluxgate magnetometer has sensitivity = 80 kV/T and bandwidth = 100 Hz. Calibration was made by rotating the axis of sensitivity in the Z component of the Earth's local geomagnetic field ( $47.5 \mu\text{T}$ ). We measured noise performance in open-loop inside a three-layer magnetic shield (Fig. 4). Also measured is the noise contribution from the sense electronics (fluxgate connected but with excitation switched off in software) and from the ADC only (ADC inputs shorted to ground). Noise spectral density is calculated using Welch's method<sup>22</sup> from a 5 min data sample at an ADC sample rate of 200 Hz. From Fig. 4, the fluxgate magnetometer noise spectral density =  $5 pT_{rms}/\sqrt{\text{Hz}} @ 1 \text{ Hz}$ . The equivalent magnetic flux noise spectral density of the sense electronics =  $1.5 pT_{rms}/\sqrt{\text{Hz}} @ 1 \text{ Hz}$  and for the 32-bit ADC =  $0.4 pT_{rms}/\sqrt{\text{Hz}} @ 1 \text{ Hz}$ .

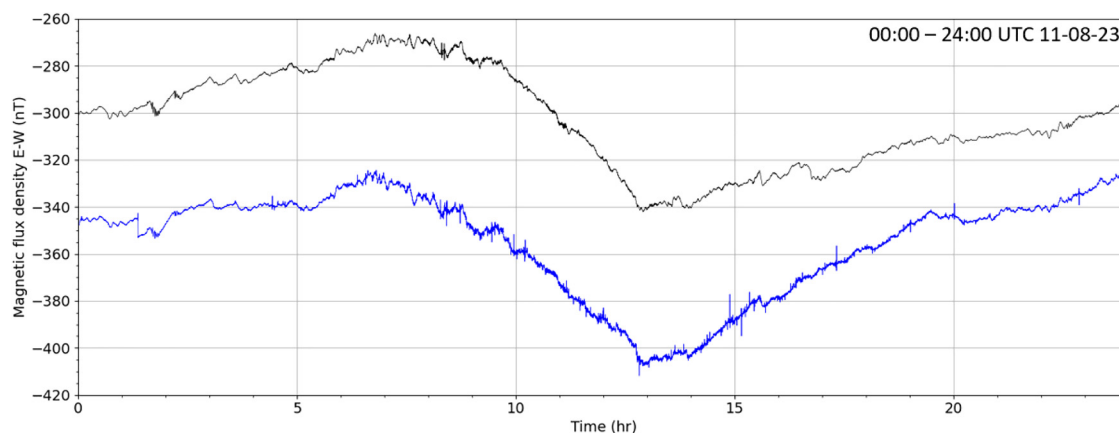


**FIG. 5.** Earth's geomagnetic field in the East-West direction (Y component) on August 11, 2023. The comparison is between our fluxgate magnetometer (blue line – 0.45 Hz cadence) in a suburban test location and the BGS Eskdalemuir observatory low-noise LEMI-025 fluxgate magnetometer (black line – 1 Hz cadence). Our magnetic flux density dataset has a y axis offset of +70 nT applied to display both datasets on this scale.

18 January 2024 16:40:50

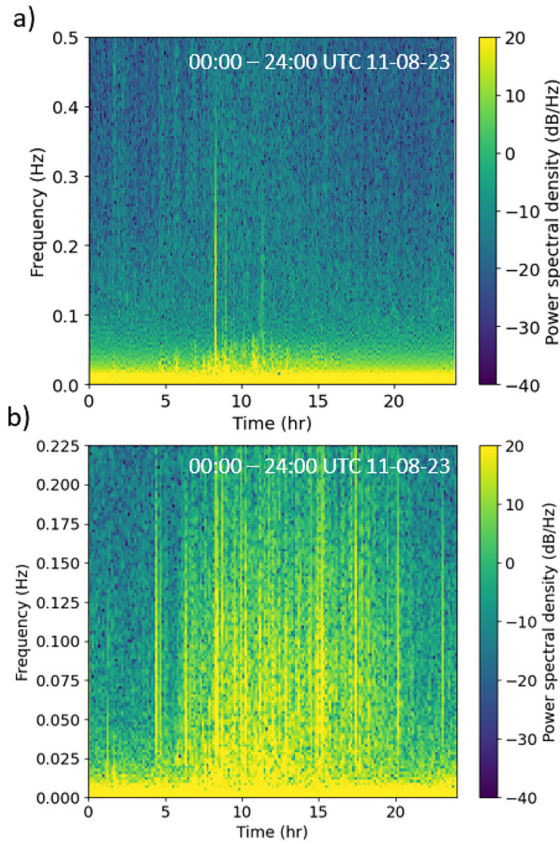


**FIG. 6.** Power spectral density spectrograms of the Earth's geomagnetic field data in Fig. 5: (a) BGS Eskdalemuir and (b) our fluxgate magnetometer in a suburban test location. There are short time windows overnight where the anthropogenic magnetic noise at our suburban test location is at a level close to that of BGS Eskdalemuir.

#### IV. GEOMAGNETIC FIELD TESTING

Low-noise fluxgate magnetometers are used to monitor the Earth's geomagnetic field at approximately 200 INTERMAGNET standard observatories around the world.<sup>23–25</sup> In addition to their remote locations, selected to minimize anthropogenic magnetic noise, geomagnetic observatories are pre-screened for magnetic anomalies and include passive or active temperature compensation.

Making geomagnetic measurements in the presence of anthropogenic magnetic noise presents a challenge; however, it has been demonstrated that useful measurements are possible from a suburban location.<sup>23,26</sup> Such capability may lead to new understanding about how the Earth's geomagnetic field changes over regions smaller than currently covered by dedicated magnetic observatories.<sup>23</sup>

Our suburban test location is 10 m from housing and contains mains power magnetic noise. The fluxgate magnetometer illustrated in Fig. 3 is located at ground level on a concrete floor of high thermal mass, alignment is made using a compass and spirit levels. The fluxgate magnetometer is mains powered using a micro-USB mobile phone charger. Magnetic flux density data are recorded and sent over WiFi by the micro-controller at a cadence of 0.45 Hz to a cloud server. The data are uncorrected for any local temperature changes.

Results are compared (Fig. 5) over a 24 h timeframe with data from the nearest British Geological Survey (BGS) observatory at Eskdalemuir, 120 km distant. Our suburban test location results in higher anthropogenic magnetic noise than BGS Eskdalemuir, including variable amplitude fast spikes due to moving vehicles. However, the ionospheric diurnal variation of the Earth's geomagnetic field is clearly visible along with faster geomagnetic field changes at the nT level, which may be due to local variations from the magnetosphere.

From a comparison of power spectral density spectrograms (Fig. 6), our data from a suburban location show broadband daytime noise approximately 20 dB higher than BGS Eskdalemuir. It also highlights short time windows overnight where the

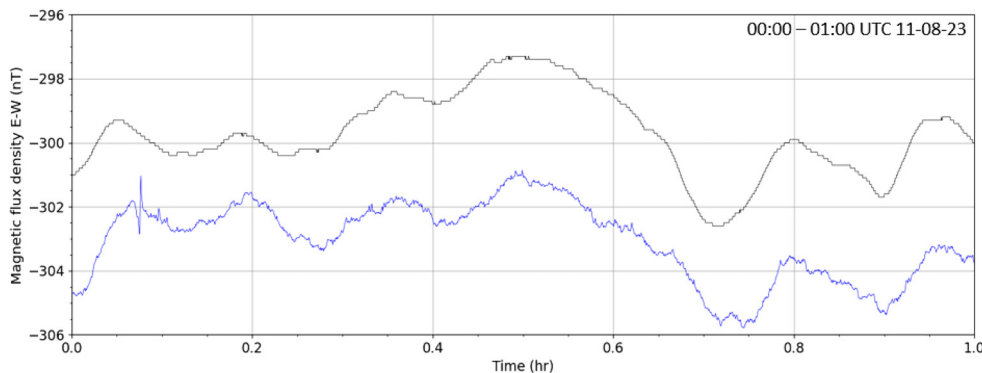


**FIG. 7.** The first hour of the data in Fig. 5. This is a period of low anthropogenic magnetic noise at our suburban test location (Fig. 6). Our prototype fluxgate magnetometer (blue line) successfully tracks the BGS Eskdalemuir observatory fluxgate magnetometer (black line) with sub-nT resolution. Our magnetic flux density dataset has a y axis offset of +113 nT applied to display both datasets on this scale.

18 January 2024 16:40:50

anthropogenic magnetic noise at our suburban test site becomes comparable with BGS Eskdalemuir. A dataset comparison during one such time window is shown in Fig. 7, where our prototype fluxgate magnetometer successfully tracks the BGS Eskdalemuir observatory fluxgate magnetometer (data truncated to 0.1 nT by BGS for historical reasons) with sub-nT resolution.

## V. CONCLUSIONS

We have developed a parallel rod fluxgate magnetometer in a single PCB of size  $5 \times 12$  cm, weight 45 g, and sensor head average power dissipation = 40 mW. The magnetic flux noise spectral density in open-loop =  $5 pT_{rms}/\sqrt{\text{Hz}}$  @ 1 Hz, sensitivity = 80 kV/T, and bandwidth = 100 Hz.

Our 0.1 Hz noise (Fig. 4) is approximately  $2 \times$  higher than the INTERMAGNET 1 s standard.<sup>24</sup> However, the fluxgate magnetometer performance level is sufficient to demonstrate sub-nT tracking of the Y component of the Earth's geomagnetic field from a suburban test location.

In addition to geomagnetic applications, there is demand for such a low-noise sensor in industrial applications, e.g., as a current mapping diagnostic tool to optimize the safety, performance, and lifetime of EV batteries.

Future work will focus on the development of fully integrated open and closed-loop fluxgate magnetometers with noise spectral density  $< 1 pT_{rms}/\sqrt{\text{Hz}}$  @ 1 Hz that also meet the INTERMAGNET 1 s standard. Testing of multiple sensor heads will be undertaken to determine the performance spread associated with the Aichi-Steel amorphous wire cores.

## ACKNOWLEDGMENTS

The authors would like to thank Gary Kendall, Ciarán Beggan, John McFadden, Iain Chalmers, and Marcin Mrozowski for useful discussions. The results presented in this paper rely on the data collected at Eskdalemuir observatory. We thank British Geological Survey for supporting its operation and INTERMAGNET for promoting high standards of magnetic observatory practice ([www.intermagnet.org](http://www.intermagnet.org)). This work was funded in part by a Faraday Institution Industrial Fellowship for T. Dyer in partnership with CDO<sup>2</sup> Ltd, Sussex Innovation Centre, Science Park Square, Brighton BN1 9SB, UK.

## AUTHOR DECLARATIONS

### Conflict of Interest

The authors have no conflicts to disclose.

### Author Contributions

**T. Dyer:** Conceptualization (lead); Data curation (lead); Formal analysis (equal); Funding acquisition (equal); Investigation (equal); Methodology (equal); Writing – original draft (lead); Writing – review & editing (equal). **P. F. Griffin:** Conceptualization (equal); Funding acquisition (equal); Project administration (equal); Resources (equal); Supervision (equal); Writing – review & editing (equal). **E. Riis:** Conceptualization (equal); Formal analysis (equal); Funding acquisition (equal); Project administration (lead);

Resources (lead); Supervision (lead); Validation (equal); Writing – review & editing (equal).

## DATA AVAILABILITY

The data that support the findings of this study are openly available from the University of Strathclyde KnowledgeBase at <https://doi.org/10.15129/f2c59f69-a82a-41f2-a068-77b07e2607c8>, Ref. 27.

## REFERENCES

- <sup>1</sup>F. Primdahl, "The fluxgate magnetometer," *J. Phys. E: Sci. Instrum.* **12**, 241 (1979).
- <sup>2</sup>P. Ripka, "Review of fluxgate sensors," *Sens. Act.* **33**, 129–141 (1992).
- <sup>3</sup>V. Korepanov and A. Marusenkov, "Flux-gate magnetometers design peculiarities," *Surv. Geophys.* **33**, 1059–1079 (2012).
- <sup>4</sup>T. Bergmark, "Experience of geomagnetic field recording with a fluxgate magnetometer having a bridge sensor," *Geophys. Surv.* **6**, 381–391 (1984).
- <sup>5</sup>O. V. Nielsen, J. R. Petersen, F. Primdahl, P. Brauer, B. Hernando, A. Fernández, J. M. G. Merayo, and P. Ripka, "Development, construction and analysis of the "Ørsted" fluxgate magnetometer," *Meas. Sci. Technol.* **6**, 1099–1115 (1995).
- <sup>6</sup>H. O'Brien, P. Brown, T. Beek, C. Carr, E. Cupido, and T. Oddy, "A radiation tolerant digital fluxgate magnetometer," *Meas. Sci. Technol.* **18**, 3645–3650 (2007).
- <sup>7</sup>T. J. Peters, "Automobile navigation using a magnetic flux-gate compass," *IEEE Trans. Veh. Technol.* **VT-35**, 41–47 (1986).
- <sup>8</sup>Y. Hu, G. Z. Iwata, M. Mohammadi, E. V. Silletta, A. Wickenbrock, J. Blanchard, D. Budker, and A. Jerschow, "Sensitive magnetometry reveals inhomogeneities in charge storage and weak transient internal currents in Li-ion cells," *Proc. Natl. Acad. Sci. U.S.A.* **117**, 10667–10672 (2020).
- <sup>9</sup>M. F. Snoeij, V. Schaffer, S. Udayashankar, and M. V. Ivanov, "Integrated fluxgate magnetometer for use in isolated current sensing," *IEEE J. Solid-State Circ.* **51**, 1684–1694 (2016).
- <sup>10</sup>M. G. Bason, T. Coussens, M. Withers, C. Abel, G. Kendall, and P. Krüger, "Non-invasive current density imaging of lithium-ion batteries," *J. Power Sources* **533**, 231312 (2022).
- <sup>11</sup>D. W. Lee, M. Eissa, A. Gabrys, B. Shulver, E. Mazotti, S. Lavangkul, S. Chevacharoenkul, N. Murphy, F. Wang, Y. Zhang, W. French, M. Jenson, and R. Jackson, "Fabrication and performance of integrated fluxgate for current sensing applications," *IEEE Trans. Mag.* **53**(11), 4004204 (2017).
- <sup>12</sup>H. Bittel, "Noise of ferromagnetic materials," *IEEE Trans. Mag.* **3**, 359 (1969).
- <sup>13</sup>M. Janosek, *Smart Sensors, Measurement and Instrumentation—High Sensitivity Magnetometers* (Springer, 2017), Chap. 2, pp. 41–62.
- <sup>14</sup>M. Janosek, M. Butta, M. Dressler, E. Saunderson, D. Novotny, and C. Fourier, "1 pT noise fluxgate magnetometer for geomagnetic measurements and unshielded magnetocardiography," *IEEE Trans. Inst. Meas.* **69**, 2552 (2020).
- <sup>15</sup>M. Butta, *Smart Sensors, Measurement and Instrumentation—High Sensitivity Magnetometers* (Springer, 2017), Chap. 3, pp. 63–102.
- <sup>16</sup>M. Dressler, M. Janosek, and M. Butta, "Reduction of magnetic noise limits of orthogonal fluxgate sensor," *AIP Adv.* **11**, 015347 (2021).
- <sup>17</sup>D. Brisinda, P. Fenici, and R. Fenici, "Clinical magnetocardiography: The unshielded bet—past, present, and future," *Front. Cardiovasc. Med.* **10**, 1232882 (2023).
- <sup>18</sup>P. Ripka and K. Závěta, *Magnetic Sensors and Magnetometers*, 2nd ed. (Artech House, 2021), Chap. 1, pp. 1–27.
- <sup>19</sup>See [https://www.aichi-steel.co.jp/\\_assets/dl/products\\_development/products/Magnetic\\_Amorphous\\_Wire.pdf](https://www.aichi-steel.co.jp/_assets/dl/products_development/products/Magnetic_Amorphous_Wire.pdf) for product datasheet.
- <sup>20</sup>M. H. Acuna, "Fluxgate magnetometers for outer planets exploration," *IEEE Trans. Mag.* **10**, 519–523 (1974).

- <sup>21</sup>S. C. Tang, M. C. Duffy, P. Ripka, and W. G. Hurley, “Excitation circuit for fluxgate sensor using saturable inductor,” *Sens. Actuators A* **113**, 156–165 (2004).
- <sup>22</sup>P. D. Welch, “The use of fast Fourier transform for the estimation of power spectra: A method based on time averaging over short, modified periodograms,” *IEEE Trans. Audio Electroacoust.* **AU-15**, 70–73 (1967).
- <sup>23</sup>C. Beggan and S. Marple, “Building a Raspberry Pi school magnetometer network in the UK,” *Geosci. Commun.* **1**, 25–34 (2018).
- <sup>24</sup>G. Wang, C. Beggan, and C. Turbitt, “Merging fluxgate and induction coil data collected from Eskdalemuir geophysical observatory to produce low-noise, one-second data,” Multi-Hazards and Resilience Programme Internal Report IR/22/020, British Geological Survey (2020).
- <sup>25</sup>P. Ripka and K. Závěta, *Magnetic Sensors and Magnetometers*, 2nd ed. (Artech House, 2021), Chap. 9, pp. 292–294.
- <sup>26</sup>M. Janosek, M. Butta, M. Vlk, and T. Bayer, “Improving Earth’s magnetic field measurements by numerical corrections of thermal drifts and man-made disturbances,” *J. Sens.* **218**, 1 (2018).
- <sup>27</sup>T. Dyer, “Data for: ‘Single-board low-noise fluxgate magnetometer,’” dataset (University of Strathclyde, 2023). <https://doi.org/10.15129/f2c59f69-a82a-41f2-a068-77b07e2607c8>